



OPEN ACCESS

EDITED BY

Dylan J.H.A. Henssen,
University Hospital Leipzig, Germany

REVIEWED BY

Bharat Hosur,
Armed Forces Medical College, Pune, India
Xin Ge,
Lanzhou University, China

*CORRESPONDENCE

Georg Gühr
✉ ggühr@gmx.de

RECEIVED 22 October 2025

REVISED 19 December 2025

ACCEPTED 07 January 2026

PUBLISHED 29 January 2026

CITATION

Gühr G, Henkes H, Khanafer A, Allouche M, Ganslandt O, Müller SJ, Wohlgemuth WA and Schob S (2026) Association between histogram parameters of T2 weighted MRI data, WHO grade, tumor proliferation index and selected molecular markers in low-grade glioma.

Front. Radiol. 6:1730316.

doi: 10.3389/fradi.2026.1730316

COPYRIGHT

© 2026 Gühr, Henkes, Khanafer, Allouche, Ganslandt, Müller, Wohlgemuth and Schob. This is an open-access article distributed under the terms of the [Creative Commons Attribution License \(CC BY\)](https://creativecommons.org/licenses/by/4.0/). The use, distribution or reproduction in other forums is permitted, provided the original author(s) and the copyright owner(s) are credited and that the original publication in this journal is cited, in accordance with accepted academic practice. No use, distribution or reproduction is permitted which does not comply with these terms.

Association between histogram parameters of T2 weighted MRI data, WHO grade, tumor proliferation index and selected molecular markers in low-grade glioma

Georg Gühr^{1*}, Hans Henkes¹, Ali Khanafer¹, Mehdi Allouche¹, Oliver Ganslandt², Sebastian Johannes Müller³, Walter Alexander Wohlgemuth⁴ and Stefan Schob⁴

¹Clinic for Neuroradiology, Katharinenhospital Stuttgart, Stuttgart, Germany, ²Clinic for Neurosurgery, Katharinenhospital Stuttgart, Stuttgart, Germany, ³Clinic for Neuroradiology, University Hospital Magdeburg, Magdeburg, Germany, ⁴Department for Radiology, University Hospital Halle (Saale), Halle (Saale), Germany

Introduction: Conventional T2 weighted MRI sequences are part of the standard diagnostics in case of LGG and implemented in every MRI protocol for the first anatomical evaluation. Despite the excellent tissue contrast and spatial information, conventional radiological assessment of these images lacks the capacity of providing reliable information about underlying histopathology. Therefore, this retrospective investigation aimed to assess whole-tumor histogram analysis (HA) of T2 weighted MRI sequences for its ability to distinguish between WHO grade 1 and 2 gliomas, to predict the isocitrate dehydrogenase 1 (IDH 1) gene mutation and the methylguanine-DNA methyl-transferase (MGMT) promoter methylation status, to differentiate oligodendrogliomas from diffuse astrocytomas, and to predict the proliferative potential using the Ki-67 proliferation index.

Methods: Signal intensities of T2 weighted pre-surgical MRI data of 53 LGG patients were used for histogram-profiling. WHO-grade, Ki-67 expression, IDH 1 mutation and MGMT promoter methylation status were evaluated. Comparative and correlative statistics were used to investigate possible associations between HA parameters and neuropathology.

Results: Statistically significant distinctions between WHO grade 1 and grade 2 gliomas were observed for T2 SI Entropy ($p = 0.001$). Furthermore, T2 SI Entropy was significantly higher in IDH 1-mutated gliomas ($p = 0.015$) and correlated significantly with the Ki-67 proliferation index ($r = 0.341$, $p = 0.019$). Noteworthy distinctions between gliomas with MGMT promoter methylation and those without were discerned for S_{min} ($p = 0.019$). No significance could be detected comparing SI histogram parameters between oligodendrogliomas and diffuse astrocytomas.

Conclusion: Our investigation demonstrates the potential of T2 SI Entropy in distinguishing grade 1 from grade 2 gliomas and in reflecting the proliferative activity denoted by Ki-67 expression, therefore being a promising HA feature for assessing tumor heterogeneity.

KEYWORDS

histogram analysis, histopathology, imaging biomarker, low-grade glioma, T2 weighted imaging, tumor heterogeneity

1 Introduction

Gliomas represent a heterogeneous group of primary central nervous system (CNS) tumors arising from glial cells, encompassing astrocytic, oligodendroglial, and ependymal subtypes, with diverse histopathological and molecular characteristics. In contrast to non-CNS neoplasms the classification and prognosis of gliomas are regularly determined by World Health Organization (WHO) grading, integrating histopathologic characteristics, biological tumor behavior and increasingly molecular biomarkers (1). Low-grade gliomas (LGG), categorized as WHO grade 1 and 2, typically manifest relatively slow growth and a less aggressive clinical course compared to high-grade gliomas (HGG, WHO grade 3 and 4). Subtypes within LGG include pilocytic astrocytoma, diffuse astrocytoma, and oligodendroglioma, collectively constituting approximately 15%–16% of all primary brain tumors (2).

Conventional anatomical magnetic resonance imaging (MRI) sequences, namely T2, fluid-attenuated inversion recovery (FLAIR) and T1 weighted images (pre- and post-contrast) are the first-line technique in terms of identifying the location of the tumor and its expansion into adjacent brain areas (3). Nevertheless, conventional MRI images are often morphologically ambivalent among the different LGG subtypes, even when using gadolinium-based contrast agents, and their routinely applied qualitative radiological assessment does not reliably allow to draw conclusions about the underlying histopathology. To overcome this limitation advanced MRI techniques such as diffusion weighted imaging (DWI), perfusion weighted imaging (PWI) and MR spectroscopy (MRS) have been long used in addition to routine anatomical evaluation (4) and especially assessed in a quantitative approach they helped to improve the diagnostic accuracy (5).

A frequently used method for such a quantitative evaluation of MRI data is histogram analysis (HA), a statistical technique to examine the distribution of data values within a dataset. By analyzing the shape and other characteristics of the MRI data histogram, represented by different histogram parameters, it is possible to gain valuable insights into the underlying tissue properties, thereby enhancing the MRI assessment of tumor heterogeneity (6). Numerous histogram-based investigations, especially of advanced MRI data such as DWI and PWI, have been presented in recent years with promising results in terms of predicting tumor grade, estimating the proliferative activity of the lesion at hand and delivering further prognostic information (7–19). Notably, studies have demonstrated that HA, even when applied to conventional anatomical MRI sequences, is capable of offering indications of biological tumor characteristics and histopathology across different tumor entities (20–25). This observation underscores the potential for HA parameters to be MRI sequence independent biomarkers. But before routinely integrating them as a component within a contemporary quantitative approach, not only applying to advanced MRI data but also to widely available conventional sequences, further investigations to clarify which of these HA parameters are the most promising need to be conducted.

Therefore, the objective of this retrospective investigation was to assess the capacity of whole tumor HA of T2 weighted MRI sequences to i) distinguish between WHO grade 1 and WHO grade 2 gliomas, ii) anticipate the isocitrate dehydrogenase 1 (IDH 1) mutation and methylguanine-DNA methyl-transferase (MGMT) promoter methylation status, iii) differentiate oligodendrogliomas from diffuse astrocytomas, and iv) predict the proliferative potential of the neoplasms, as indicated by the Ki-67 proliferation index.

2 Materials and methods

2.1 Patients

Our institutional Radiological Information System (RIS) was systematically searched for patients diagnosed with low-grade glioma and primary brain tumors. A total of 61 patients, who underwent diagnostic biopsy or surgical removal of tumors with subsequent neuropathological assessment within our hospital between January 2012 and January 2017 were identified. Tumor classification and grading was conducted according to the 2016 WHO classification of CNS tumors. Inclusion criteria mandated patients to have undergone pretreatment Magnetic Resonance Imaging (MRI) scans with sufficient T2 weighted imaging data. Patients with an artificial image data set, mostly due to motion related artifacts, or patients with intratumoral hemorrhage were excluded.

Ultimately, 53 patients qualified for our retrospective analysis, comprising 11 pilocytic astrocytomas WHO 1, 31 diffuse astrocytomas WHO 2 and 11 oligodendrogliomas WHO 2.

The WHO 1 pilocytic astrocytoma group consisted of 5 females and 6 males, with a mean age of 24 years. The WHO 2 diffuse astrocytoma group comprised 15 females and 16 males, with a mean age of 41 years. In the WHO 2 oligodendroglioma group were 5 females and 6 males with a mean age of 43 years. Among the cohort, 33 patients exhibited an IDH 1 mutation, while 15 patients had an IDH 1 wildtype status (IDH 1 mutation status was unavailable for 5 patients). MGMT promoter methylation was observed in 23 patients, and 11 patients presented with an unmethylated MGMT promoter (MGMT promoter methylation status was unavailable for 19 patients). 4 patients lacked available Ki-67 proliferation index data and were consequently excluded from the correlation analysis.

2.2 MRI protocol

All patients received a brain MRI scan using a 1.5T device (MAGNETOM Aera or MAGNETOM Symphony Tx/Rx CP head coil, Siemens, Erlangen, Germany). 47 out of 53 patients were examined with the MAGNETOM Area system using the same protocol and set of parameters. The imaging protocol included the following sequence:

Axial T2 weighted (T2w) turbo spin echo (TSE) sequence (TR/TE: 5390/99, flip angle: 150°, slice thickness: 5 mm, acquisition matrix: 512 × 291, field of view: 230 × 187 mm).

All digitalized MRI images were analyzed by two experienced radiologists (DHR, SS) on a PACS workstation (Impax EE R20 XII).

2.3 Histogram analysis of T2 SI volumes

T2 weighted turbo spin echo (TSE) images were extracted from our institutional archive in Digital Imaging and Communications in Medicine (DICOM) format through the aforementioned AGFA PACS. Subsequently, comprehensive lesion histogram profiling was conducted using a DICOM image analysis tool developed by N.G. using MATLAB (The Mathworks, Natick, MA, USA). In the MATLAB function histogram, the bin width was determined using the auto setting, which is based on the Freedman–Diaconis rule. No additional normalization or interpolation was performed. T2 weighted images were loaded into a graphical user interface (GUI) to annotate the neoplastic lesions in each patient across all respective MRI sections. The tumor segmentation process was manually performed in consensus by two experienced neuroradiologists. Cystic components and adjacent edema were excluded.

The entire lesion histogram profile of T2 signal intensities (SI) was then systematically calculated, yielding a comprehensive set of parameters, including SImean, SImin, SImax, SIp10, SIp25, SIp75, SIp90, SImodus, SImedian, SI standard deviation (SD), Skewness, Kurtosis, and Entropy.

2.4 Neuropathology

All tumor specimens underwent neuro-histological verification of the diagnosis. Tumor samples, acquired through stereotactic biopsy, partial, or complete resection, were subjected to formalin fixation and paraffin embedding for subsequent histopathologic diagnostics, immunohistochemistry, and polymerase chain reaction (PCR) sequencing. The embedded samples were sectioned at a thickness of 3 µm and stained with hematoxylin and eosin (H&E).

Immunohistochemistry involved the use of specific antibodies against IDH1-R132H (dilution 1:20, product no. DIA-H09; Dianova, Hamburg, Germany) and Ki67 (dilution 1: 800; M7240; Dako Denmark A/S, Glostrup, Denmark). Histopathological images were digitized using a Leica microscope equipped with a DFC290 HD digital camera and LAS V4.4 software (Leica Microsystems, Wetzlar, Germany). Sections designated for immunohistochemistry and PCR sequencing underwent histological analysis to ascertain the presence of viable tumor infiltration while ensuring the absence of necrotic areas and hemorrhage. A positive result for IDH 1 immunohistochemistry was determined by strong cytoplasmic staining. The tumor proliferation index was calculated by dividing the number of specifically stained (Ki-67 positive) cell

nuclei by the total number of nuclei, with the area displaying the highest number of positive cell nuclei selected in each case.

Fluorescence *in situ* Hybridization (FISH) was used to detect 1p/19q codeletion using dual-color probes targeting 1p36/1q25 and 19q13/19p13.

For the assessment of the MGMT gene's methylation status, tumor DNA was isolated from micro-dissected 10 µm-thick sections from paraffin-embedded tissue blocks using the Maxwell[®] RSC FFPE Plus DNA Kit AS1720 (Promega, Madison, WI, USA) and the Maxwell[®] RSC Instrument (Promega). The isolated DNA underwent bisulfite treatment using the EpiTect[®] Bisulfite Kit (QIAGEN, Hilden, Germany) following the manufacturer's procedures. The bisulfite-converted DNA was then amplified in a PCR reaction, and the methylation status was determined by pyrosequencing using the Therascreen MGMT Pyro[®] Kit (QIAGEN), targeting 4 CpG islands (chromosome 10, Exon 1, range 131265519–131265537, CGACGCCCGCAGGTCCTCG). A methylation percentage of 10% or higher was considered positive for methylation.

2.5 Statistical analysis

Statistical analyses, including graphical representation, were conducted utilizing GraphPad Prism 9 (GraphPad Software, San Diego, CA, USA). In the initial phase, a comprehensive examination of T2 SI data and histopathological information was undertaken through descriptive statistics. Subsequently, Gaussian distribution of the data was assessed using the Shapiro–Wilk Test. A T-Test was executed to compare normally distributed parameters derived from T2 SI histogram profiling between WHO 2 and WHO 2 gliomas. Additionally, unpaired T-Tests were employed to compare normally distributed T2 SI histogram profiling parameters between IDH 1-mutated and IDH 1-wildtype gliomas, between MGMT promoter-methylated and unmethylated gliomas as well as between oligodendrogliomas and diffuse astrocytomas. For parameters exhibiting a non-Gaussian distribution, Mann–Whitney-U Tests were conducted.

Correlation analyses for normally distributed parameters utilized the Pearson Correlation Coefficient, while Spearman-Rho Rank-Order Correlation was employed in cases of non-Gaussian distribution.

A significance threshold of *p*-values < 0.05 was universally adopted.

Finally, the accuracy of T2 SI histogram profiling was assessed through receiver operating characteristics (ROC) curve analysis. The corresponding area under the curve (AUC) was calculated, and Youden's Index was determined for parameters with optimal test accuracy to estimate potential cut-off values.

3 Results

Figure 1 depicts illustrative instances of cranial MRI scans obtained from individuals diagnosed with WHO grade 1

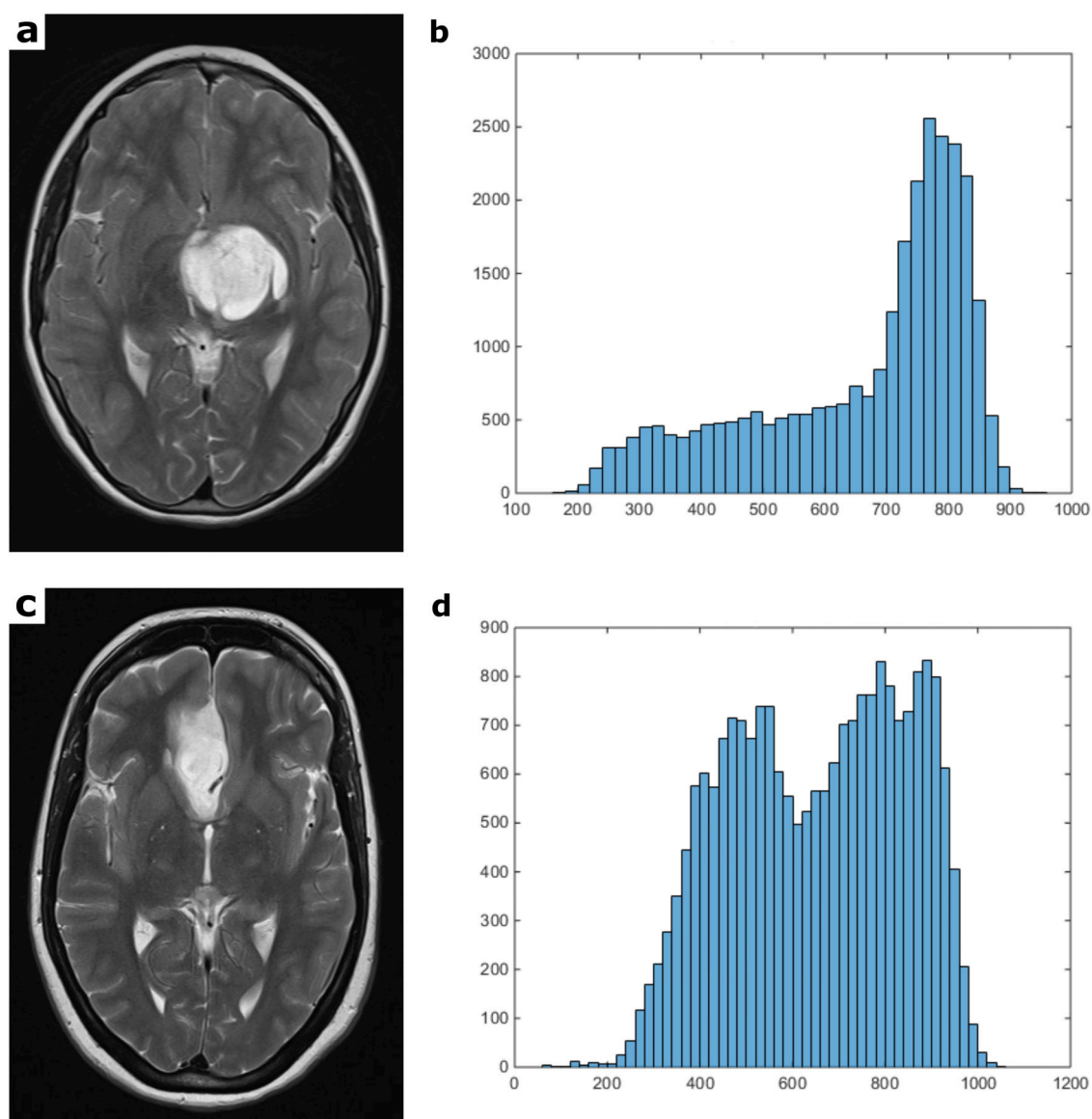


FIGURE 1

Figure 1 compares representative T2 weighted MRI sections and the corresponding whole tumor SI histogram of a grade 1 (a,b) and a grade 2 glioma (c,d). The first image of the upper case shows a T2 weighted turbo-spin-echo (TSE) sequence of a pilocytic astrocytoma (WHO grade 1), located in the left thalamus with moderate mass effect and midline crossing (a). The first image of the lower case displays a T2 weighted TSE sequence of a diffuse astrocytoma (WHO grade 2) originating from the right mesial frontal lobe (c). These images are good examples of MRI-morphological similarities often found between different tumor entities, which makes further histopathological classification using conventional radiological assessment impossible. The second images of each row show the T2 SI histograms (b,d; x-axis: SI values in incremental order, y-axis: number of voxels).

astrocytoma (upper case) and WHO grade 2 astrocytoma (lower case). Additionally, the corresponding histograms of the whole tumor T2 signal intensities (SI) are presented in the respective image series.

The findings of the descriptive analysis of T2 SI data, tumor volumes, and Ki-67 proliferation index for all examined gliomas are presented in Table 1.

Gaussian distribution was confirmed by Shapiro–Wilk-Test for S_{max}, S_{Ip75}, S_{Ip90}, S_{Imodus}, SI SD, Skewness, Entropy, and Ki-67. Conversely, non-Gaussian distribution was identified

for S_{mean}, S_{Imin}, S_{Ip10}, S_{Ip25}, S_{Imedian}, Kurtosis, and tumor volume.

Consequently, an (unpaired) T-Test was employed for the comparative analysis of parameters, including S_{max}, S_{Ip75}, S_{Ip90}, S_{Imodus}, SI SD, Skewness, Entropy, and Ki-67, across different categories such as grade 1 and grade 2 gliomas, IDH 1 mutation-positive and negative gliomas, MGMT promoter methylated and unmethylated gliomas, as well as between oligodendrogliomas and diffuse astrocytomas. Whereas, the Mann–Whitney-U Test was utilized to assess the statistical

TABLE 1 Tumor volume, SI histogram parameters and Ki-67 proliferation index of all investigated gliomas.

Parameters	Mean ± Standard deviation	Minimum	Maximum
Lesion volume × 10 ³ mm ³	50.87 ± 59.00	0.72	212.51
SI _{mean}	682.40 ± 186.70	374.80	1,193.00
SI _{min}	177.98 ± 120.35	1	567
SI _{max}	1,085.34 ± 273.52	557	1,866
SI _{P10}	484.52 ± 120.53	278	854
SI _{P25}	577.37 ± 155.67	312	996
SI _{P75}	788.97 ± 227.61	428	1,448
SI _{P90}	859.27 ± 240.62	466	1,582
Median	694.58 ± 208.54	356	1,268
Mode	725.98 ± 250.58	203	1,365
Standard deviation	145.06 ± 59.37	44.12	329.30
Kurtosis	3.03 ± 1.52	1.80	11.78
Skewness	-0.06 ± 0.64	-1.29	1.95
Entropy	5.01 ± 0.76	3.26	6.11
Ki-67%	4.55 ± 2.31	1	10

TABLE 2 Comparison of SI histogram parameters, Ki-67 index and lesion volume between WHO grade 1 and grade 2 gliomas.

Parameters	WHO I °	WHO II °	p-values
	Mean ± SD	Mean ± SD	
Lesion volume × 10 ³ mm ³	25.58 ± 31.60	58.38 ± 63.40	0.040
SI _{mean}	733.01 ± 191.89	669.19 ± 185.38	0.318
SI _{min}	239.36 ± 168.78	161.90 ± 100.73	0.172
SI _{max}	1,133.73 ± 254.21	1,072.67 ± 279.87	0.515
SI _{P10}	503.78 ± 119.07	479.47 ± 121.60	0.492
SI _{P25}	621.80 ± 148.65	565.74 ± 157.09	0.292
SI _{P75}	847.73 ± 246.68	773.58 ± 222.92	0.341
SI _{P90}	912.71 ± 263.27	845.27 ± 235.71	0.413
Median	762.45 ± 227.23	676.81 ± 202.50	0.229
Mode	793.01 ± 262.94	708.40 ± 247.49	0.321
Standard deviation	159.30 ± 78.08	141.33 ± 53.99	0.377
Kurtosis	3.80 ± 2.76	2.83 ± 0.93	0.227
Skewness	-0.09 ± 0.05	-0.04 ± 0.58	0.863
Entropy	4.37 ± 0.88	5.18 ± 0.64	0.001
Ki-67%	2.5 ± 1.65	5.11 ± 2.16	<0.001

Statistically significant p-values are given in bold.

differences in parameters SI_{mean}, SI_{min}, SI_{P10}, SI_{P25}, SI_{median}, Kurtosis, and tumor volume among the specified groups.

Statistically significant distinctions between WHO grade 1 and grade 2 gliomas were observed for T2 SI Entropy (*p* = 0.001), tumor volume (*p* = 0.04) and Ki-67 proliferation index (*p* < 0.001). The mean values of T2 SI Entropy, tumor volume, and Ki-67 proliferation index were all markedly lower in the WHO grade I group.

Comparison of T2 SI histogram profiles of IDH 1 mutated and IDH 1 wildtype gliomas revealed significant differences for Entropy (*p* = 0.015), with higher values in case of mutated IDH 1. Whereas a subgroup analysis comparing IDH 1 mutated and IDH 1 wildtype gliomas within the WHO grade 2 cohort revealed no statistical significance (*p* = 0.281).

Moreover, noteworthy distinctions between gliomas with MGMT promoter methylation and those without were discerned for SI_{min} (*p* = 0.019), exhibiting an elevation in unmethylated gliomas.

TABLE 3 Comparison of SI histogram parameters between IDH 1 mutated and IDH 1 wildtype gliomas.

Parameters	IDH 1 mutation	IDH wildtype	p-values
	Mean ± SD	Mean ± SD	
SI _{mean}	675.0 ± 165.0	711.7 ± 227.3	0.530
SI _{min}	159.8 ± 105.2	213.7 ± 150.8	0.159
SI _{max}	1,079.0 ± 242.9	1,109 ± 348.0	0.732
SI _{P10}	488.5 ± 116.7	501.5 ± 140.2	0.730
SI _{P25}	573.2 ± 144.9	597.2 ± 179.75	0.624
SI _{P75}	777.6 ± 195.8	827.1 ± 281.2	0.485
SI _{P90}	844.0 ± 199.5	914.59 ± 309.5	0.347
Median	684.5 ± 180.3	719.5 ± 250.0	0.584
Mode	717.9 ± 228.5	750.5 ± 296.1	0.679
Standard deviation	138.9 ± 43.5	156.0 ± 78.5	0.336
Kurtosis	2.88 ± 01.00	2.87 ± 0.79	0.965
Skewness	-0.09 ± 0.62	-0.001 ± 0.46	0.366
Entropy	5.22 ± 0.62	4.65 ± 0.92	0.015
Entropy (WHO II °)	5.23 ± 0.63	4.95 ± 0.74	0.281

Statistically significant p-values are given in bold.

On the other hand, no significance could be detected comparing SI histogram parameters between oligodendrogliomas and diffuse astrocytomas.

For the sake of comprehensibility and clarity, the outcomes of the comparative statistical analyses are succinctly presented in Tables 2–5.

Figures 2a–c provides box plots illustrating significant SI histogram profile parameters related to WHO grade, IDH I mutation, and MGMT methylation status.

Potential associations among SI_{max}, SI_{P75}, SI_{P90}, SI_{modus}, SI SD, Skewness, Entropy, and Ki-67 were explored through the calculation of Pearson’s Correlation Coefficient. Spearman-Rho Rank-Order Correlation was employed to investigate potential associations between SI_{mean}, SI_{min}, SI_{P10}, SI_{P25}, SI_{median}, Kurtosis, and Ki-67. A significant, albeit moderate, correlation was observed between Ki-67 and Entropy (*r* = 0.341, *p* = 0.019). The comprehensive results of the correlative analyses are summarized in Table 6.

Additionally, the scatter plot graphically depicting the association between T2 SI Entropy and Ki-67 is presented in Figure 2d.

Moreover, Area Under the Curve (AUC) values were computed for each of the assessed parameters that demonstrated statistically significant differences. The obtained values, along with their confidence intervals (CI), are as follows: SI Entropy WHO 1 vs. 2 (AUC = 0.775, [CI: 0.608–0.942], $p = 0.005$), SI Entropy IDH 1 mutated vs. wildtype (AUC = 0.677, [CI: 0.504–0.850], $p = 0.052$), SImin MGMT methylated vs. unmethylated (AUC = 0.715, [CI: 0.539–0.892], $p = 0.045$). The corresponding Receiver Operating Characteristic (ROC) curves are presented in Figure 3.

Finally, Youden’s Index for SI Entropy was calculated to determine the most promising cutoff value for distinguishing WHO grade 1 and 2 gliomas, revealing an Entropy value of 4.99 and above to indicate WHO grade 2 with a sensitivity of 69.05% and a specificity of 81.82%.

TABLE 4 Comparison of SI histogram parameters between MGMT methylated and MGMT unmethylated gliomas.

Parameters	MGMT methylated	MGMT unmethylated	p-values
	Mean ± SD	Mean ± SD	
SI _{mean}	699.5 ± 215.5	746.3 ± 176.2	0.536
SI _{min}	144.8 ± 114.1	258.0 ± 146.6	0.019
SI _{max}	1,108.1 ± 319.1	1,181.64 ± 269.0	0.514
SI _{P10}	498.4 ± 138.0	539.4 ± 133.4	0.419
SI _{P25}	592.0 ± 181.0	624.7 ± 151.4	0.608
SI _{P75}	811.0 ± 259.6	857.6 ± 211.6	0.608
SI _{P90}	881.7 ± 271.3	945.3 ± 221.1	0.504
Median	710.6 ± 238.1	751.7 ± 194.6	0.623
Mode	750.2 ± 282.4	772.27 ± 270.3	0.830
Standard deviation	146.2 ± 59.7	161.5 ± 55.2	0.479
Kurtosis	2.74 ± 00.56	3.09 ± 1.52	0.971
Skewness	−0.12 ± 0.49	0.18 ± 0.73	0.201
Entropy	5.21 ± 0.73	4.82 ± 0.71	0.151

Statistically significant p-values are given in bold.

4 Discussion

In this retrospective investigation we systematically analyzed T2 weighted MRI images, using a quantitative approach by histogram profiling, to elucidate potential applications in the *in-vivo* classification of tumor grades and the prediction of prognostically relevant molecular parameters. Not surprisingly, we detected significant differences in the comparative statistical analysis between WHO grade 1 and grade 2 gliomas concerning Ki-67 proliferation index and tumor volume with higher volume and higher proliferative activity in the grade 2 group, as estimating the proliferation is part of the pathological grading system and a higher proliferation rate inevitably leads to faster tumor growth.

As introduced above, a histogram is a graphical representation of the frequency distribution of a dataset. It provides a visual summary of the data, making it easier to identify specific patterns or characteristics. Different parameters are routinely used in the context of HA to describe the data characteristics. There are those, which reflect the center and location of the histogram in the data continuum like median, mean, mode, minimum, maximum and the percentiles, sometimes referred as first order parameters and those indicating the shape and spread of the histogram like skewness, kurtosis and entropy, sometimes called second order parameters. First order histogram characteristics have the same unit as the investigated variable, in our case T2 signal intensity, and thus depend directly on the measured values. For example, higher T2 signal of the respective tumor inevitably leads to higher first order histogram parameters in general, regardless of the morphological tumor structure and tumor heterogeneity. Second order histogram characteristics, on the other hand, are unit independent. They represent different aspects of the data distribution independently of the absolute values and should therefore be more suitable for the assessment of tumor heterogeneity using conventional T2 weighted MRI images. This postulation is in line with the present study results of the comparative statistics. None of the first order characteristics achieved significance between grade 1 and grade 2 gliomas, whereas T2 SI Entropy as second order histogram

TABLE 5 Comparison of SI histogram parameters between WHO 2 oligodendrogliomas and diffuse astrocytomas.

Parameters	Oligodendrogliomas	Diffuse Astrocytomas	p-values
	Mean ± SD	Mean ± SD	
SI _{mean}	612.77 ± 112.84	689.21 ± 202.83	0.245
SI _{min}	183.09 ± 85.28	154.39 ± 10,592.8	0.493
SI _{max}	1,030 ± 212.81	1,087.81 ± 301.74	0.616
SI _{P10}	451 ± 83.16	489.57 ± 132.30	0.372
SI _{P25}	521 ± 100.97	581.61 ± 171.26	0.276
SI _{P75}	703.55 ± 130.33	798.42 ± 244.57	0.230
SI _{P90}	769.55 ± 129.92	872.14 ± 259.72	0.219
Median	616 ± 126.34	698.39 ± 221.10	0.251
Mode	658.73 ± 151.69	726.03 ± 273.52	0.445
Standard deviation	122.05 ± 25.27	148.18 ± 59.88	0.171
Kurtosis	2.73 ± 0.58	2.87 ± 1.03	0.888
Skewness	−0.01 ± 0.41	−0.06 ± 0.63	0.822
Entropy	5.12 ± 0.55	5.20 ± 0.68	0.733

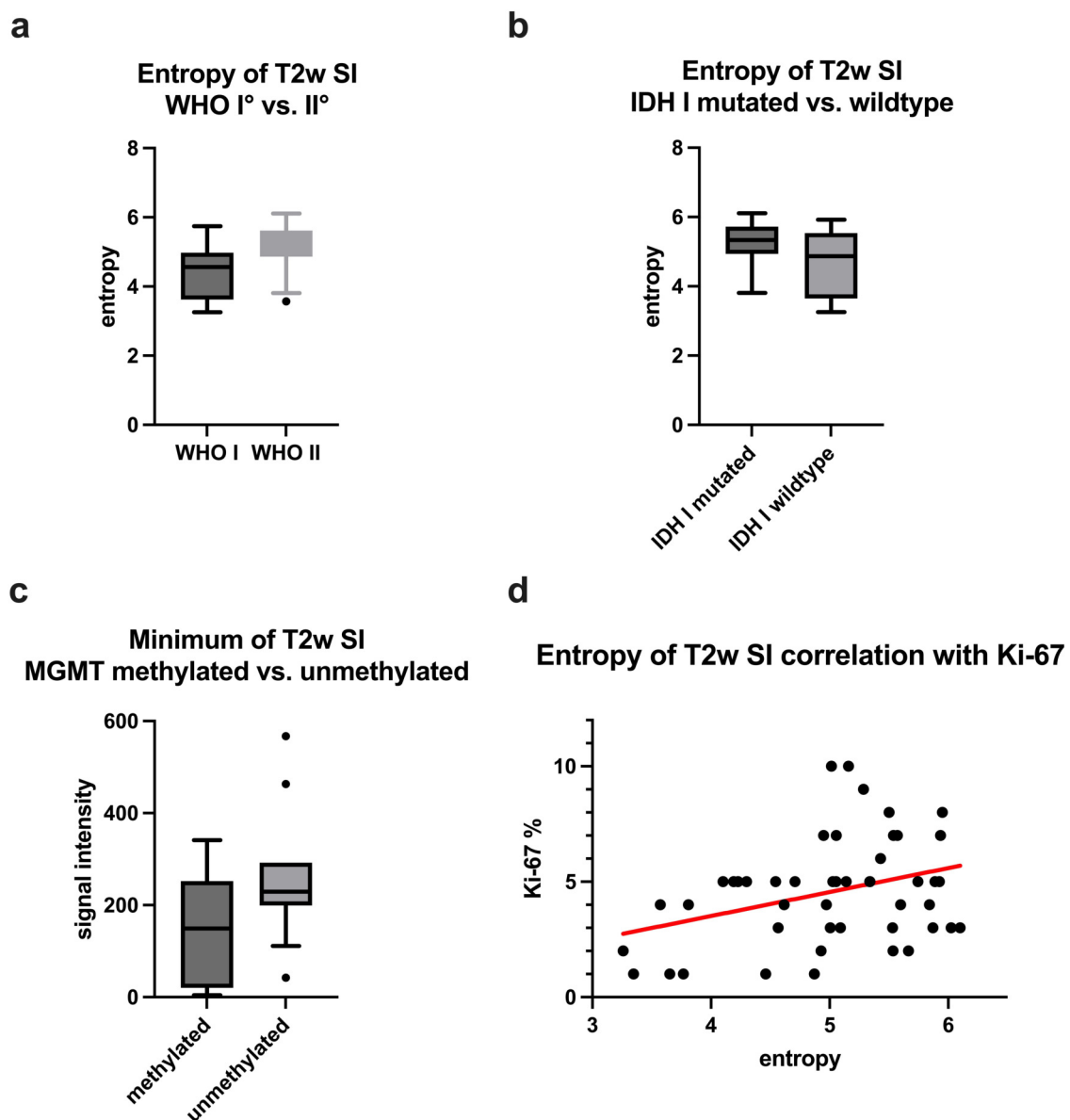


FIGURE 2

Figure 2 provides boxplots of statistically significant differences between the T2 SI entropy of grade 1 and grade 2 gliomas (a) and of IDH 1 mutated and IDH 1 wildtype gliomas (b). A boxplot demonstrating the significant difference of T2 SI minimum between MGMT promoter methylated and unmethylated gliomas is displayed in (c). The last image (d) shows a moderate correlation between T2 SI entropy and the proliferation index Ki-67.

parameter was significantly lower in the grade 1 group, with strong significance ($p = 0.001$). Similar results have been presented in previous studies, showing histogram Entropy to be increased in case of higher tumor grades and malignant neoplasia (13, 14, 26–30). In the context of histogram analysis, entropy is a measure of the randomness or disorder in a distribution of data values. It can be used to quantify the amount of information or uncertainty in a histogram. The entropy (H) of a discrete probability distribution is typically computed using the formula:

$$H(x) = - \sum_{i=1}^n P(x_i) \times \log_2(P(x_i)),$$

where n is the number of intensity levels in the histogram and $P(x_i)$ is the probability of occurrence of the i -th intensity level. Entropy is high when the distribution is more uniform or when there is no dominant intensity level, indicating greater uncertainty. On the other hand, low entropy suggests a more peaked or concentrated distribution with less uncertainty. Applied to our case of T2 weighted MRI images, this would mean that the entropy would be minimal if the measured lesion had only a single signal intensity (for example an idealized homogenous cyst). In contrast, the more morphologically complex and diverse the lesion, consisting of many different signal intensities without a concentration of individual intensities, the higher the corresponding T2 SI entropy would be. Understanding these

underlying mathematical principles and transferring them to HA of MRI data, one must conclude that particularly histogram entropy should be a very suitable parameter for assessing the heterogeneity of a lesion. This conclusion is also supported by

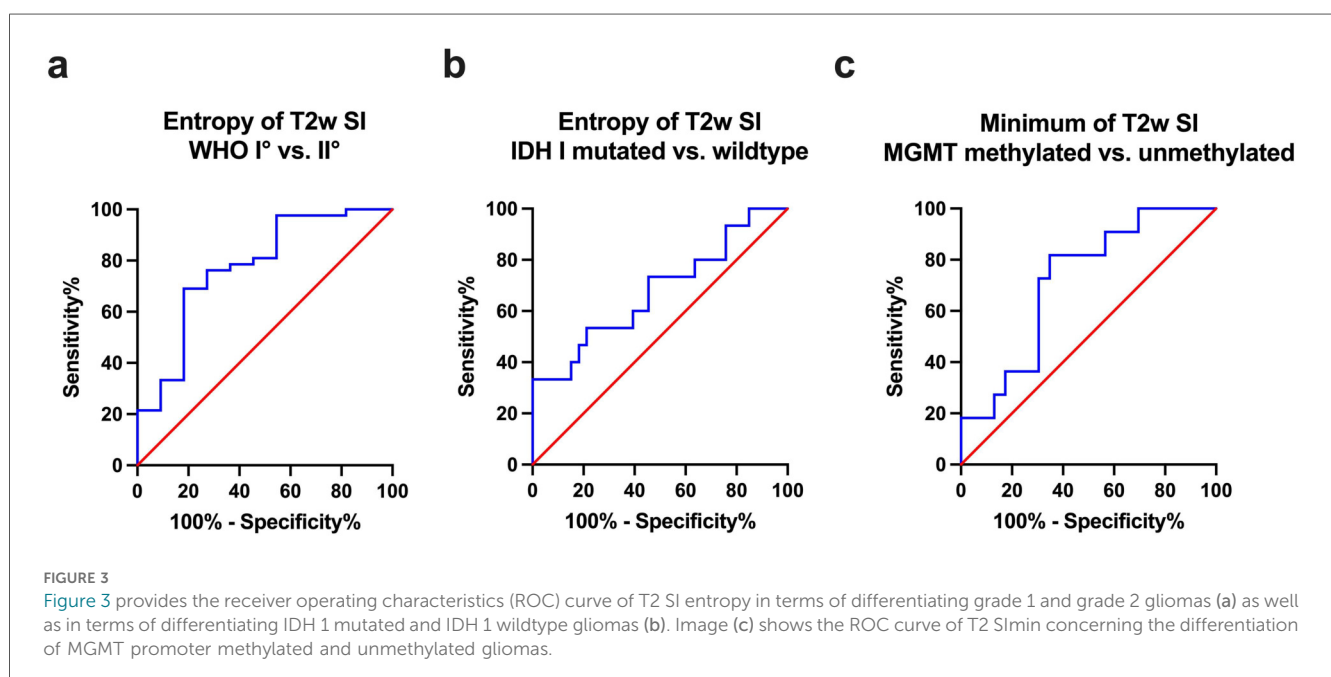
the study results of the statistical correlation analysis, in which the T2 SI entropy correlates positively with the proliferation index Ki-67 ($r = 0.341, p = 0.019$). Since the tumor grade is by definition directly linked to the mitotic activity of the tumor tissue and higher proliferation in turn leads to increased tissue heterogeneity, we consider the correlation between entropy and Ki-67 to be further confirmation of the assumption that entropy could be a possible heterogeneity marker. A number of recent studies have also demonstrated a statistical correlation between the histogram entropy of various MRI data and the proliferation index Ki-67, thus supporting this hypothesis (13, 15, 20, 31–33).

TABLE 6 Correlations between SI histogram parameters and Ki-67 in all investigated gliomas.

Parameters	Ki-67
SI _{mean}	$r = -0.179$
	$p = 0.216$
SI _{min}	$r = -0.147$
	$p = 0.315$
SI _{max}	$r = -0.004$
	$p = 0.980$
SI _{P10}	$r = -0.135$
	$p = 0.355$
SI _{P25}	$r = -0.165$
	$p = 0.258$
SI _{P75}	$r = -0.195$
	$p = 0.180$
SI _{P90}	$r = -0.196$
	$p = 0.177$
Median	$r = -0.177$
	$p = 0.221$
Mode	$r = -0.156$
	$p = 0.286$
Standard deviation	$r = -0.181$
	$p = 0.214$
Kurtosis	$r = 0.107$
	$p = 0.465$
Skewness	$r = 0.101$
	$p = 0.490$
Entropy	$r = 0.341$
	$p = \mathbf{0.019}$

Statistically significant p -values are given in bold.

In this study we also investigated whether HA of T2 SI enables the prediction of the IDH 1 mutation and the MGMT promoter methylation status of the respective glioma. Protein-truncating mutation in isocitrate dehydrogenase 1 (IDH 1) or in isocitrate dehydrogenase 2 (IDH 2) is associated with a more favorable outcome and a longer overall survival in case of low-grade astrocytomas and oligodendroglial tumors (34–36). In addition, methylation of the promoter of O-6-methylguanine-DNA methyltransferase (MGMT) gene limits the ability of the tumor cells to repair DNA damage caused by chemotherapy and radiation, resulting in increased survival time (37–39). In the comparative statistics we detected significant higher T2 SI entropy values in the IDH 1 mutant group compared to the wildtype group, even though the ROC analysis was not quite significant. Since all grade 1 gliomas in our study cohort were pilocytic astrocytomas and they usually do not carry mutations in the IDH 1 gene (in our investigation only one out of eleven) and the major part of the grade 2 glioma cohort were IDH 1 mutants (42 IDH 1 mutants vs. 8 IDH 1 wildtypes) and thus comparing IDH 1 wildtype with IDH 1 mutant in our study effectively means comparing grade 1 with grade 2 glioma, we believe this result not to be an independent effect of the IDH 1 mutation status but



rather an overlapping effect of the tumor grade. The subgroup analysis, comparing IDH 1 mutant and IDH 1 wildtype glioma within the WHO grade 2 cohort, supported this suspicion, although the probability of a type II error is likely to be relatively high due to the small number of grade 2 IDH wildtype tumors (8 in total). Furthermore, MGMT promoter methylated gliomas showed significantly lower minimal T2 signal intensities (SI_{min}) in contrast to unmethylated entities. Interestingly, a similar result was obtained in a previous histogram study for the MGMT status of LGG concerning minimum values of apparent diffusion coefficient (ADC) (14). The MGMT promoter methylated LGG in this study had significant lower ADC_{min} values compared to the unmethylated gliomas and it was also the only histogram parameter that reached significance in the comparative statistics. Nevertheless, as there are no other histogram studies of simple MRI signal intensities in gliomas, especially not with investigation of the MGMT promoter methylation status, it is not yet possible to assess whether the SI_{min} values represent a true MGMT promoter methylation status-dependent phenotype. Furthermore, it must also be taken into account that the MRI images were not normalized, which may have influenced the results of the first-order HA parameters. Further studies with bigger samples and normalized SI datasets are needed in this context to clarify the significance of this finding.

Additionally, we compared T2 SI histogram parameters of grade 2 glioma with and without codeletion of chromosomal arms 1p and 19q. None of the HA parameters achieved statistical significance in this context. But this result could be due to the relatively low number of oligodendrogliomas in this study (12 in total) with consequently high probability for false negative results. Whether this result is a reflection of the possibly comparable tumor heterogeneity on the micro- and macroscopic scale cannot be confirmed with certainty based on the results of this study.

Our study exhibits certain limitations that warrant consideration. Primarily, it is characterized as a retrospective investigation with a relatively small number of patients, especially in the subgroups, and thus potentially statistically underpowered. Therefore, the non-significant results can only be interpreted to a limited extent. It should also be mentioned that, due to the exploratory nature of this study, we combined circumscribed and diffuse gliomas in our cohort and thus used the term “low-grade glioma” in a broader sense compared to the latest edition of the WHO classification of tumors of the CNS from 2021. Additionally, the exclusive availability of data derived from 1.5-Tesla MRI systems inherently results in diminished signal-to-noise ratios within the MRI data. This necessitates the acquisition of MRI images with a reduced pixel matrix, consequently leading to a diminution in spatial information when compared to examinations with a higher field strength. Also, the acquisition of T2 images with a slice thickness of 5 mm could alter the histogram caused by partial volume effects at the tumor margins. Moreover, due to partially missing data of the patient sample, especially concerning the MGMT-methylation status, statistical bias and therefore lower statistical power and accuracy may have occurred in these instances. Furthermore, related to the preliminary nature of our

investigation, the familywise alpha inflation due to serial hypothesis tests in the statistical analysis was not controlled.

Finally, it was only a single center study using MRI devices from the same manufacturer. Although the vast majority of patients were examined using the same MRI scanner, further studies are required to clarify whether the type of MRI device and manufacturer as well as the examination parameters have an influence on the histogram parameters and thus to validate the robustness and reliability of the HA of simple morphological MRI data as method to assess tumor heterogeneity.

5 Conclusion

Histogram profiling of T2 weighted morphological MRI data encompasses the derivation of first and second order characteristics through distinct parameters. Our investigation demonstrates the potential of T2 SI entropy as second order parameter in distinguishing grade 1 from grade 2 gliomas and in reflecting the proliferative activity denoted by Ki-67 expression. We postulate that entropy, in particular, is a promising HA parameter in terms of assessing tumor heterogeneity and should be subject of further imaging studies. For example, it is quite conceivable that entropy could also be a suitable parameter as part of an AI-supported approach with appropriately trained deep neural networks.

Data availability statement

The original contributions presented in the study are included in the article/Supplementary Material, further inquiries can be directed to the corresponding author.

Ethics statement

The studies involving humans were approved by Ethik-Kommission Landesärztekammer Baden-Württemberg, F-2017-047. The studies were conducted in accordance with the local legislation and institutional requirements. The human samples used in this study were acquired from a by-product of routine care or industry. Written informed consent for participation was not required from the participants or the participants' legal guardians/next of kin in accordance with the national legislation and institutional requirements.

Author contributions

GG: Conceptualization, Data curation, Formal analysis, Investigation, Project administration, Writing – original draft, Writing – review & editing. HH: Resources, Writing – review & editing. AK: Formal analysis, Writing – review & editing. MA: Data curation, Writing – review & editing. OG: Writing – review & editing. SM: Data curation, Writing – review &

editing. WW: Writing – review & editing. SS: Conceptualization, Investigation, Project administration, Software, Supervision, Writing – original draft, Writing – review & editing.

Funding

The author(s) declared that financial support was not received for this work and/or its publication.

Conflict of interest

The author(s) declared that this work was conducted in the absence of any commercial or financial relationships that could be construed as a potential conflict of interest.

The author SS declared that they were an editorial board member of *Frontiers*, at the time of submission. This had no impact on the peer review process and the final decision.

References

- Louis DN, Perry A, Wesseling P, Brat DJ, Cree IA, Figarella-Branger D, et al. The 2021 WHO classification of tumors of the central nervous system: a summary. *Neuro-Oncol.* (2021) 23:1231–51. doi: 10.1093/neuonc/noab106
- Ostrom QT, Price M, Neff C, Cioffi G, Waite KA, Kruchko C, et al. CBTRUS Statistical report: primary brain and other central nervous system tumors diagnosed in the United States in 2015–2019. *Neuro-Oncol.* (2022) 24:v1–v95. doi: 10.1093/neuonc/noac202
- Fouke SJ, Benzinger T, Gibson D, Ryken TC, Kalkanis SN, Olson JJ. The role of imaging in the management of adults with diffuse low grade glioma: a systematic review and evidence-based clinical practice guideline. *J. Neurooncol.* (2015) 125:457–79. doi: 10.1007/s11060-015-1908-9
- Bulakbaş N, Paksoy Y. Advanced imaging in adult diffusely infiltrating low-grade gliomas. *Insights Imaging.* (2019) 10:122. doi: 10.1186/s13244-019-0793-8
- Caulo M, Panara V, Tortora D, Mattei PA, Briganti C, Pravata E, et al. Data-Driven grading of brain gliomas: a multiparametric MR imaging study. *Radiology.* (2014) 272:494–503. doi: 10.1148/radiol.14132040
- Just N. Improving tumour heterogeneity MRI assessment with histograms. *Br J Cancer.* (2014) 111:2205–13. doi: 10.1038/bjc.2014.512
- Schob S, Meyer J, Gawlitza M, Frydrychowicz C, Müller W, Preuss M, et al. Diffusion-Weighted MRI reflects proliferative activity in primary CNS lymphoma. *PLoS One.* (2016) 11:e0161386. doi: 10.1371/journal.pone.0161386
- Woo S, Cho JY, Kim SY, Kim SH. Histogram analysis of apparent diffusion coefficient map of diffusion-weighted MRI in endometrial cancer: a preliminary correlation study with histological grade. *Acta Radiol. Stockh. Swed.* 1987. (2014) 55:1270–7. doi: 10.1177/0284185113514967
- Surov A, Gottschling S, Mawrin C, Prell J, Spielmann RP, Wienke A, et al. Diffusion-Weighted imaging in meningioma: prediction of tumor grade and association with histopathological parameters. *Transl. Oncol.* (2015) 8:517–23. doi: 10.1016/j.tranon.2015.11.012
- Schob S, Meyer HJ, Dieckow J, Pervinder B, Pazaitis N, Höhn A, et al. Histogram analysis of cervical cancer aids detecting lymphatic metastases—a preliminary study. *Mol. Imaging Biol.* (2017) 19:953–62. doi: 10.1007/s11307-017-1073-y
- Surov A, Ginat DT, Lim T, Cabada T, Baskan O, Schob S, et al. Histogram analysis parameters apparent diffusion coefficient for distinguishing high and low-grade meningiomas: a multicenter study. *Transl. Oncol.* (2018) 11:1074–9. doi: 10.1016/j.tranon.2018.06.010
- Gühr G, Horvath-Rizea D, Garnov N, Kohlhof-Meinecke P, Ganslandt O, Henkes H, et al. Diffusion profiling via a histogram approach distinguishes low-grade from high-grade meningiomas, can reflect the respective proliferative

Generative AI statement

The author(s) declared that generative AI was not used in the creation of this manuscript.

Any alternative text (alt text) provided alongside figures in this article has been generated by *Frontiers* with the support of artificial intelligence and reasonable efforts have been made to ensure accuracy, including review by the authors wherever possible. If you identify any issues, please contact us.

Publisher's note

All claims expressed in this article are solely those of the authors and do not necessarily represent those of their affiliated organizations, or those of the publisher, the editors and the reviewers. Any product that may be evaluated in this article, or claim that may be made by its manufacturer, is not guaranteed or endorsed by the publisher.

potential and progesterone receptor Status. *Mol. Imaging Biol.* (2018) 20:632–40. doi: 10.1007/s11307-018-1166-2

14. Gühr G, Horvath-Rizea D, Hekeler E, Ganslandt O, Henkes H, Hoffmann KT, et al. Histogram analysis of diffusion weighted imaging in low-grade gliomas: *in vivo* characterization of tumor architecture and corresponding neuropathology. *Front. Oncol.* (2020) 10:206. doi: 10.3389/fonc.2020.00206

15. Gühr G, Horvath-Rizea D, Hekeler E, Ganslandt O, Henkes H, Hoffmann KT, et al. Diffusion weighted imaging in high-grade gliomas: a histogram-based analysis of apparent diffusion coefficient profile. *PLoS One.* (2021) 16:e0249878. doi: 10.1371/journal.pone.0249878

16. Gühr G, Horvath-Rizea D, Kohlhof-Meinecke P, Ganslandt O, Henkes H, Härtig W, et al. Diffusion weighted imaging in gliomas: a histogram-based approach for tumor characterization. *Cancers (Basel).* (2022) 14:3393. doi: 10.3390/cancers14143393

17. Ma X, Ren X, Shen M, Ma F, Chen X, Zhang G, et al. Volumetric ADC histogram analysis for preoperative evaluation of LVSI Status in stage I endometrioid adenocarcinoma. *Eur. Radiol.* (2022) 32:460–9. doi: 10.1007/s00330-021-07996-6

18. Bozdağ M, Er A, Çinkoğlu A. Histogram analysis of ADC maps for differentiating brain metastases from different histological types of lung cancers. *Can. Assoc. Radiol. J. J. Assoc. Can. Radiol.* (2021) 72:271–8. doi: 10.1177/0846537120933837

19. Su Y, Kang J, Lin X, She D, Guo W, Xing Z, et al. Whole-Tumor histogram analysis of diffusion and perfusion metrics for noninvasive pediatric glioma grading. *Neuroradiology.* (2023) 65:1063–71. doi: 10.1007/s00234-023-03145-6

20. Gühr GA, Horvath-Rizea D, Kohlhof-Meinecke P, Ganslandt O, Henkes H, Richter C, et al. Histogram profiling of postcontrast T1-weighted MRI gives valuable insights into tumor biology and enables prediction of growth kinetics and prognosis in meningiomas. *Transl. Oncol.* (2018) 11:957–61. doi: 10.1016/j.tranon.2018.05.009

21. Meyer HJ, Schob S, Münch B, Frydrychowicz C, Garnov N, Quäschling U, et al. Histogram analysis of T1-weighted, T2-weighted, and postcontrast T1-weighted images in primary CNS lymphoma: correlations with histopathological findings—a preliminary study. *Mol. Imaging Biol.* (2018) 20:318–23. doi: 10.1007/s11307-017-1115-5

22. Meyer HJ, Leifels L, Hamerla G, Höhn AK, Surov A. Histogram analysis parameters derived from conventional T1- and T2-weighted images can predict different histopathological features including expression of Ki67, EGFR, VEGF, HIF-1 α , and P53 and cell count in head and neck squamous cell carcinoma. *Mol. Imaging Biol.* (2019) 21:740–6. doi: 10.1007/s11307-018-1283-y

23. Meyer HJ, Hamerla G, Höhn AK, Surov A. Whole lesion histogram analysis derived from morphological MRI sequences might be able to predict EGFR- and Her2-expression in cervical cancer. *Acad. Radiol.* (2019) 26:e208–15. doi: 10.1016/j.acra.2018.09.008

24. Li X, Miao Y, Han L, Dong J, Guo Y, Shang Y, et al. A. Meningioma grading using conventional MRI histogram analysis based on 3D tumor measurement. *Eur. J. Radiol.* (2019) 110:45–53. doi: 10.1016/j.ejrad.2018.11.016
25. Xue C, Zhou Q, Zhang P, Zhang B, Sun Q, Li S, et al. MRI Histogram analysis of tumor-infiltrating CD8+ T cell levels in patients with glioblastoma. *NeuroImage Clin.* (2023) 37:103353. doi: 10.1016/j.nicl.2023.103353
26. Li H, Zhao S, Fan HY, Li Y, Wu XP, Miao YP. The effect of histogram analysis of DCE-MRI parameters on differentiating renal tumors. *Clin. Lab.* (2023) 69(11). doi: 10.7754/Clin.Lab.2023.221126
27. Xiang S, Ren J, Xia Z, Yuan Y, Tao X. Histogram analysis of dynamic contrast-enhanced magnetic resonance imaging in the differential diagnosis of parotid tumors. *BMC Med. Imaging.* (2021) 21:194. doi: 10.1186/s12880-021-00724-y
28. Wang Q, Zhang L, Li S, Sun Z, Wu X, Zhao A, et al. Histogram analysis based on apparent diffusion coefficient maps of bone marrow in multiple myeloma: an independent predictor for high-risk patients classified by the revised international staging system. *Acad. Radiol.* (2022) 29:e98–e107. doi: 10.1016/j.acra.2021.07.010
29. Ren J, Yuan Y, Tao X. Histogram analysis of diffusion-weighted imaging and dynamic contrast-enhanced MRI for predicting occult lymph node metastasis in early-stage oral tongue squamous cell carcinoma. *Eur. Radiol.* (2022) 32:2739–47. doi: 10.1007/s00330-021-08310-0
30. Liu X, Han T, Wang Y, Liu H, Sun Q, Xue C, et al. Whole-Tumor histogram analysis of postcontrast T1-weighted and apparent diffusion coefficient in predicting the grade and proliferative activity of adult intracranial ependymomas. *Neuroradiology.* (2024) 66(4):531–41. doi: 10.1007/s00234-024-03319-w
31. Guo Y, Kong QC, Li LQ, Tang WJ, Zhang WL, Ning GY, et al. Whole volume apparent diffusion coefficient (ADC) histogram as a quantitative imaging biomarker to differentiate breast lesions: correlation with the ki-67 proliferation Index. *BioMed Res. Int.* (2021) 2021:4970265. doi: 10.1155/2021/4970265
32. Wang S, Zhao Z, Zhang Y, Yang L, Huang Y, Ruan Y, et al. Quantitative perfusion histogram parameters of dynamic contrast-enhanced MRI to identify different pathological types of uterine leiomyoma. *Zhejiang Xue Xue Bao Yi Xue Ban J. Zhejiang Univ. Med. Sci.* (2021) 50:97–105. doi: 10.3724/zdxbyxb-2021-0036
33. Zhou Q, Jin J, Wang Y, Wang Y, Wang T, Zhang H, et al. Dynamic contrast-enhanced magnetic resonance imaging in epithelial ovarian tumor categorization: comparison with apparent diffusion coefficient histogram analysis and the tumor cell proliferation marker. *Am. J. Transl. Res.* (2023) 15:1862–70.
34. The Cancer Genome Atlas Research Network Comprehensive, Integrative Genomic Analysis of Diffuse Lower-Grade Gliomas. *N. Engl. J. Med.* (2015) 372:2481–98. doi: 10.1056/NEJMoa1402121
35. Ceccarelli M, Barthel FP, Malta TM, Sabedot TS, Salama SR, Murray BA, et al. Molecular profiling reveals biologically discrete subsets and pathways of progression in diffuse glioma. *Cell.* (2016) 164:550–63. doi: 10.1016/j.cell.2015.12.028
36. Yan H, Parsons DW, Jin G, McLendon R, Rasheed BA, Yuan W, et al. IDH1 And IDH2 mutations in gliomas. *N. Engl. J. Med.* (2009) 360:765–73. doi: 10.1056/NEJMoa0808710
37. Hegi ME, Liu L, Herman JG, Stupp R, Wick W, Weller M, et al. Correlation of O 6-methylguanine methyltransferase (MGMT) promoter methylation with clinical outcomes in glioblastoma and clinical strategies to modulate MGMT activity. *J. Clin. Oncol.* (2008) 26:4189–99. doi: 10.1200/JCO.2007.11.5964
38. Hegi ME, Diserens AC, Gorlia T, Hamou MF, De Tribolet N, Weller M, et al. MGMT Gene silencing and benefit from temozolomide in glioblastoma. *N. Engl. J. Med.* (2005) 352:997–1003. doi: 10.1056/NEJMoa043331
39. Stupp R, Hegi ME, Gilbert MR, Chakravarti A. Chemoradiotherapy in malignant glioma: standard of care and future directions. *J. Clin. Oncol.* (2007) 25:4127–36. doi: 10.1200/JCO.2007.11.8554